International Journal of Nanomedicine

Dovepress
open access to scientific and medical research

Open Access Full Text Article

ORIGINAL RESEARCH

Cetuximab-modified CuS nanoparticles integrating near-infrared-II-responsive photothermal therapy and anti-vessel treatment

This article was published in the following Dove Press journal:
International Journal of Nanomedicine

Bin Li[1]
Zhongyin Jiang[1]
Diya Xie[1]
Yiqing Wang[1]
Xingzhen Lao[2]

[1]Department of Biomedical Engineering, College of Engineering and Applied Sciences, Nanjing University, Nanjing, Jiangsu Province 210093, China; [2]Department of Microbial and Biochemical Pharmacy, School of Life Science and Technology, China Pharmaceutical University, Nanjing , Jiangsu Province 210009, China

Background: Photothermal therapy (PTT) has received extensive attention owing to its non-invasive nature and highly therapeutic outcomes. PTT agents and near-infrared (NIR) laser are essential elements in PTT. However, most PTT agents are composed of heavy metals, characterized by serious cytotoxicity and side effects, and NIR irradiation often damages normal tissue owing to the high dose, thus limiting the clinical application of PTT.

Purpose: In this regard, exploring new perspectives enabling more PTT agents to be enriched into the tumor and NIR laser irradiation decay in PTT is vital.

Methods: In this study, cetuximab (Ab), an anti-angiogenic antibody which targets the EGFR, was modified on CuS NPs (CuS-Ab NPs) to improve the aggregation of CuS NPs in the tumor.

Results: The cellular uptake data and the biodistribution results showed comparable accumulation of CuS-Ab NPs in tumor, thus decreasing the cytotoxicity and side effects in normal tissues. More importantly, the modification of Ab in CuS-Ab NPs impressively inhibited the formation and progression of tumor vessels, as demonstrated by immunohistochemistry staining. The introduction of anti-vessel treatment requires CuS-Ab NPs to provide weak PTT, which means that a small amount of laser energy is required, inevitably causing negligible damage to normal tissue.

Conclusion: Therefore, our tailor-made CuS-Ab NPs have promising potential in clinical applications.

Keywords: photothermal therapy, CuS NPs, active targeting, cetuximab, EGFR, anti-angiogenesis

Introduction

Despite the increasing and amazing advances in clinical cancer treatment, including surgery, chemotherapy, and radiotherapy, most cancer patients still suffer from tumor metastasis, recurrence, and early death.[1,2] Small invisible lesions, negligible therapeutic outcome, and devastating side effects may account for the failure of treatment. As such, it is urgently desirable to explore intelligent and powerful strategies for tumor treatment.[3,4]

Owing to its minimal invasiveness and impressive therapeutic outcome, photothermal therapy (PTT) has been investigated for many years and is increasingly regarded as a good alterative to clinical cancer treatment.[5–7] The research community has been attempting to develop a diverse range of PTT agents, among which organic-based,[8,9] gold-based,[10,11] carbon-based,[12,13] and transition metal oxide/sulfide-based[14–20] nanoparticles (NPs) are the most common. Unfortunately, these PTT agents usually feature short-wavelength absorbency, thereby greatly restricting the tissue penetration depths and maximum permissible exposure (MPE).[21–23] Near-infrared-I (NIR-I), ranging from

Correspondence: Yiqing Wang
Department of Biomedical Engineering, College of Engineering and Applied Sciences, Nanjing University, 22 Hankou Road, Nanjing, Jiangsu Province 210093, China
Email wangyiqing@nju.edu.cn

Xingzhen Lao
Department of Microbial and Biochemical Pharmacy, School of Life Science and Technology, China Pharmaceutical University, 24 Tongjiaxiang, Nanjing, Jiangsu Province 210009, China
Email lao@cpu.edu.cn

submit your manuscript | www.dovepress.com
Dovepress
http://dx.doi.org/10.2147/IJN.S175334

650 nm to 950 nm, and NIR-II, ranging from 1,000 nm to 1,350 nm, are two NIR biological windows.[24–26] Although the NIR-I window has been widely researched, the NIR-II window permits deeper tissue penetration depths and higher MPE of the laser.[23,27] However, studies concerning PTT in the NIR-II region have rarely been reported. Hence, synthesis of NIR-II laser-responsive PTT agents which are capable of achieving deeper tissue penetration depths and higher MPE is vital and remains challenging.

Furthermore, it is difficult for non-targeting ultrasmall metal NPs to act as PTT agents to achieve a long halflife and sufficient enrichment in the tumor site. On this basis, great efforts are needed to design a new system in which NIR-II laser-responsive PTT and active tumor targeting are achieved concurrently.

In this study, we tailor-made cetuximab (Ab)-modified CuS NPs (CuS-Ab NPs). Using this platform, Ab could target the EGFR, which is overexpressed on most cancer cell membranes and is responsible for tumorigenic development, angiogenesis, and metastasis.[28,29] More importantly, Ab not only functioned as a target but also suppressed the tumor growth, metastasis, and recurrence by preventing EGFR phosphorylation.[30,31] The in vitro and in vivo results showed that with the help of Ab, more CuS NPs were accumulated in tumors rather in normal tissues, and superior therapeutic outcome was achieved even under a small laser energy (0.2 W/cm^2), therefore fully demonstrating that CuS-Ab NPs are capable of effectively ablating the tumor without breaking down the normal tissues. These results provide evidence that CuS-Ab NPs have the potential for clinical application.

Materials and methods

Materials

All agents were obtained from commercial firms and were not purified again. $CuCl_2{\cdot}2H_2O$ was bought from Shanghai Xinbao Fine Chemical Factory (Shanghai, China). Fluorescein isothiocyanate–polyethylene glycol–thiol (FITC-PEG2k-SH), thioacetamide, and mercaptoacetic acid (thioglycolic acid, TGA) were obtained from Aladdin (Shanghai, China). Sodium hydroxide (NaOH) was obtained from Wanqing Chemical Glassware & Instrument Co. (Nanjing, China). N-hydroxysulfosuccinimide sodium salt (sulfo-NHS) and 1-(3-dimethylaminopropyl)-3-ethylcarbodiimide hydrochloride (EDC) were bought from Aladdin (Shanghai, China). The MTT assay, calcein-acetoxymethyl ester (calcein AM) and propidium iodide (PI) kit, annexin-V-FITC and propidium iodide (PI) kit, and other reagents (such as LysoTracker Green and DAPI) were purchased from Beyotime Institute of Biotechnology (Nanjing, China). Ab was bought from Merck Serono (Shanghai, China). All ultrapure water was Milli-Q deionized water (Millipore, 18.2 MΩ cm^{-1}).

Instrumentation

The absorption spectrum of a sample was recorded over the wavelength region from 300 nm to 1,200 nm by a UV-3600 spectrophotometer (Shimadzu, Kyoto, Japan). Changes in NP size were measured by dynamic light scattering (DLS) using a Zetasizer Nano-ZS90 (Malvern instruments Ltd., Worcs, UK). The fluorescence images of cellular uptake were obtained using an FV1000 microscope (Olympus, Tokyo, Japan). The fluorescence images of calcein AM/PI staining were obtained with an inverted fluorescence microscope (IX73; Olympus). Transmission electron microscopy (TEM) (JEM-200CX; JEOL Optical Laboratory,Tokyo, Japan) was used to observe the morphology of NPs. A CAD4/PC (Enraf-Nonius, Rotterdam, the Netherlands) was used to assess the X-ray diffraction (XRD) spectra. Inductively coupled plasma optical emission spectrometry (ICP-OES) (OPTIMA 5300 DV; PerkinElmer Inc., Waltham, MA, USA) was utilized to detect the concentration of copper. For the MTT assay, a microplate reader (Infinite® 200 Pro NanoQuant; Tecan, Männedorf, Switzerland) was used to record the absorption values. Fluorescence imaging was obtained with an IVIS Lumina XR III in vivo imaging system (PerkinElmer Inc.). A 1,064 nm laser (Xilong Scientific Co., Ltd., Shantou, China) was utilized in these experiments. A Fotric 225-1 thermal camera (Shanghai, China) was used to quantify the temperature.

Cell line and mouse model

The mouse mammary tumor cell line 4T1 cells and the human umbilical vein endothelial cells (HUVECs) were obtained from the Cell Bank of Shanghai Institutes for Biological Science (Shanghai, China). The 4T1 cells were seeded in DMEM with 10% FBS (Nanjing Keygen Biotech. Co., Nanjing, China), while the HUVECs were grown in endothelial cell growth medium-2 (EGM-2) (LonzaBasel, Switzerland) in a 37°C humidified incubator containing 5% CO_2. The 4-week-old healthy female nude mice were bought from the Comparative Medicine Center of Yangzhou University (Yangzhou, China).

Synthesis of CuS NPs

The synthesis of CuS NPs was conducted as shown in Figure 1A. In brief, 0.1 mmol $CuCl_2{\cdot}2H_2O$ was added to 100 mL ultrapure water and mixed with TGA (0.2 mmol). After stirring for 20 minutes, the pH was adjusted to 9.0 with NaOH (0.5 M). Then, 20 mL of thioacetamide (0.1 mmol) was added to the mixture. The procedure was maintained at 50°C for 6 hours and

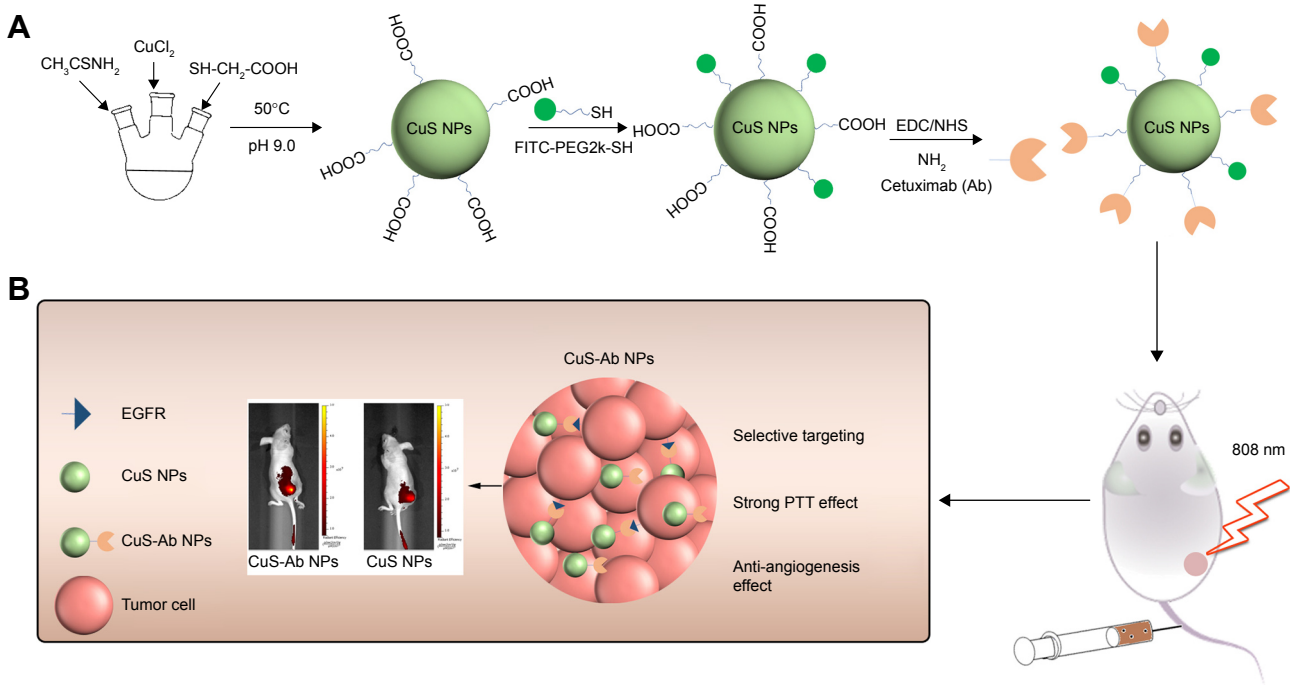

Figure 1 Scheme of synthesis and therapy of CuS-Ab NPs.
Notes: (**A**) Schematic diagram of synthesis for FITC-CuS-Ab NPs. (**B**) Illustration of CuS-Ab NPs' target tumor.
Abbreviations: CuS NP, CuS nanoparticle; CuS-Ab NP, cetuximab-modified CuS NP; EDC, 1-(3-dimethylaminopropyl)-3-ethylcarbodiimide hydrochloride; FITC, fluorescein isothiocyanate; NHS, N-hydroxysulfosuccinimide; PTT, photothermal therapy.

protected by N_2. Subsequently, the reaction was stopped and the CuS NPs were purified using ultrafiltration filters (1 kDa) in a centrifuge (8,000 rpm, 30 minutes, three times). Then, FITC-PEG2k-SH (2 mmol, 10 µL) was added to the CuS NP solution and the mixture was stirred continuously for 24 hours. Lastly, Ab (1 mL, 5 mg/mL) was functionalized on the surface of FITC-CuS NPs, which were activated by EDC and sulfo-NHS (FITC-CuS NPs:EDC:NHS =1:1.2:1.2). After stirring for another 12 hours, the FITC-CuS NPs were centrifuged to remove excess reagents and washed three times with ultrapure water. The purified FITC-CuS-Ab NPs and FITC-CuS NPs were kept at 4°C and quantified by ICP-OES.

Characterization of NPs

TEM (JEM-200CX) was used to observe the morphology of CuS NPs and CuS-Ab NPs. The difference in hydrodiameters between CuS NPs and CuS-Ab NPs was measured by a Zetasizer Nano-ZS90 and absorption spectra were monitored from 300 nm to 1,200 nm by a UV-3600 spectrophotometer. Then, to compare CuS NPs and CuS-Ab NPs, XRD spectra were recorded on a CAD4/PC. After irradiation with a 1,064 nm laser, the photothermal stability was evaluated by thermal imaging in vitro. In brief, 3 mL of NPs were injected into a quartz cell and exposed to an NIR laser (1,064 nm, 0.2 W/cm^2, 10 minutes), and temperature changes were recorded using a real-time infrared (IR) thermal camera.

In vitro cytotoxicity assay

To consider PTT combined with Ab, the anti-tumor efficacy was further evaluated in vitro. The MTT assay was used to assess the toxicity of CuS NPs and CuS-Ab NPs in HUVECs and 4T1 cells, respectively. First, the cells (2×10^3 cells in 100 µL per well) were cultured in 96-well plates with growth medium (10% FBS) at 37°C and 5% CO_2. After 12 hours, cells were washed three times with PBS and incubated with 100 µL of CuS NPs (10 µg/mL, 20 µg/mL, and 40 µg/mL, based on the concentration of copper ions), CuS NPs (10 µg/mL, 20 µg/mL, and 40 µg/mL, based on the concentration of copper ions) + Ab (41 µg/mL, based on the concentration ratio of the initial reaction), and CuS-Ab NPs (10 µg/mL, 20 µg/mL, and 40 µg/mL, based on the concentration of copper ions) for 24 hours, while the control group was left untreated. Then, the 96-well plates were washed again and MTT solution was added. After undisturbed incubation for another 4 hours in a dark field, the absorbance value of each group was measured by an Infinite 200 Pro NanoQuant microplate reader at 570 nm.

Flow cytometry and calcein AM/PI staining

To further verify the anti-tumor effect in vitro, flow cytometry and calcein AM/PI staining were employed, and the

4T1 cells (3×10^4) were cultured with DMEM (10% FBS) in six-well plates at 37°C and 5% CO_2. Then, the cells were washed three times with PBS and co-incubated with CuS NPs (1 mL, 40 μg/mL, based on copper ions), CuS NPs (1 mL, 40 μg/mL, based on copper ions) + Ab (41 μg/mL, based on the concentration ratio of the initial reaction), and CuS-Ab NPs (40 μg/mL, 1 mL, based on copper ions) for 24 hours. Then, the treatment groups were irradiated under a 1,064 nm laser (0.2 W/cm^2, 10 minutes), while the control group was left untreated. For flow cytometry, cells were split using 0.25% trypsin (free EDTA) and collected by centrifugation (1,000 rpm, 5 minutes). 4T1 cells were co-stained with annexin-V-FITC and PI and evaluated by flow cytometry according to the protocol of the apoptosis detection kit. For calcein AM/PI staining, the double-staining method was conducted for 20 minutes after cells had been washed with PBS in six-well plates. Following this, images of living and dead cells were obtained under an Olympus IX73 fluorescence microscope and analyzed using ImageJ software.

Cellular uptake of NPs

4T1 cells (1 mL, ~2×10^4 cells/mL) were incubated with DMEM and 10% FBS in a glass-bottomed dish at 37°C and 5% CO_2. After 12 hours, the tumor cells were co-cultured with FITC-CuS NPs (10 μg/mL, based on copper ions) and FITC-CuS-Ab NPs (10 μg/mL, based on copper ions) for 2 hours in a dark field. Then, cells were co-stained with LysoTracker Green and DAPI for another 15 minutes and washed three times with PBS. Cells were immediately observed under an FV1000 microscope and the fluorescence images were analyzed by ImageJ.

Scratch test

HUVECs (1×10^5 per well) were seeded into six-well plates with EGM-2 medium (10% FBS) at 37°C and 5% CO_2 for 12 hours.[32,33] A sterile pipette tip (1 mL) was used to wound the monolayer cells and denuded cells were washed with PBS. Then, cells were co-incubated with CuS NPs (1 mL, 10 μg/mL, based on copper ions), CuS NPs (1 mL, 10 μg/mL, based on copper ions) + Ab (41 μg/mL, based on the concentration ratio of the initial reaction), and CuS-Ab NPs (1 mL, 10 μg/mL, based on copper ions), while the control group was left untreated. After 24 hours, the wound of the monolayer cells was monitored under an optical microscope.

Anti-angiogenesis of CuS-Ab NPs in chick embryo chorioallantoic membrane (ECM)

Fertilized chicken eggs were purchased and co-incubated with CuS-Ab NPs at 37°C and about 70% humidity for 1 week.[34,35] In brief, the eggs were washed in 75% alcohol and a window was opened in the side of each egg in a pathogen-free environment. CuS-Ab NPs (100 μL, 10 μg/mL) were added dropwise into the ECM without destruction, while the control group received no treatment. The eggs with windows were immediately isolated to prevent infection and dehydration. After 1 week, images of the membrane of the eggs were obtained through the window.

Xenograft tumor models

The 4T1 cells (100 μL, 5×10^5 cells per mice) were inoculated subcutaneously into the right back (flank) of healthy female nude mice. The tumor-bearing mice were monitored daily and randomized into four groups when the average tumor volume reached 100 mm^3. The establishment of tumor-bearing mice and experimental procedure were conducted under pathogen-free conditions, based on the protocols of the Institutional Animal Care and Use Committee (IACUC) of Nanjing University (protocol number 20180112-011).

In vivo fluorescence imaging

Mice with tumor xenografts were prepared and injected intravenously with CuS NPs (100 μL, 10 μg/mL, based on copper ions) and CuS-Ab NPs (100 μL, 10 μg/mL, based on copper ions). After 60 minutes, fluorescence imaging in tumor-bearing mice was carried out and analyzed with the IVIS Lumina XR III in vivo imaging system. Then, the mice were killed and organs were collected. The organs were immediately imaged at an emission wavelength of 520 nm and an excitation wavelength of 488 nm.

In vivo anti-tumor effect of anti-angiogenesis combined with PTT

The mouse-derived xenograft tumor mice were assigned randomly to four groups (n=6 per group): 1) control group; 2) CuS NPs (100 μL, 10 μg/mL, based on copper ions) + laser group; 3) CuS NPs (100 μL, 10 μg/mL, based on copper ions) + Ab (41 μg/mL, based on the concentration ratio of the reaction mixture) + laser group; and 4) CuS-Ab NPs (100 μL, 10 μg/mL, based on copper ions) + laser group. All treatment groups were injected intravenously and irradiated under a 1,064 nm laser (0.2 W/cm^2, 10 minutes). The temperature of xenograft tumor mice, which were exposed to the laser, was recorded in real time using an IR thermal camera (Fotric, Shanghai, China). The tumor volume and weight of the mice were monitored every other day. After 2 weeks, the mice were killed and tissues (heart, liver, lung, spleen, kidney, and tumor) were harvested for further analysis.

Histological analysis

After the mice had been weighed and killed on the 15th day, the tissues were harvested immediately and fixed in 4% (v/v) paraformaldehyde solution for H&E staining and immunohistochemistry (IHC) staining. In brief, the tissues were dehydrated and embedded in paraffin. Then, the paraffin-embedded tissues were sectioned into 30 μm slices for H&E staining, and neovascularization in the tumor was assessed by IHC staining. The sections were observed under a light microscope and representative images were further analyzed.

Statistical analysis

Statistical analysis was conducted using a one-way ANOVA followed by a multiple-comparison Bonferroni test. All data were analyzed with at least three samples, and a *P*-value <0.05 was considered statistically significant.

Results and discussion

Synthesis and characterization

In the second NIR-II window, CuS NPs showed outstanding photothermal conversion efficiencies and low levels of damage to normal tissue.[36,37] However, these materials would accumulate in off-target organs owing to their lack of tumor-homing behavior. Ab, as an antibody, can target EGFR, which is overexpressed on 4T1 cell membranes, exhibiting excellent anti-angiogenesis properties in tumor therapy.[29,38] With the introduction of FITC-PEG2k-SH, the NPs could be traced in vitro and in vivo (Figure 1B).

The synthesis procedure of CuS-Ab NPs was performed as shown in Figure 1A. The CuS NPs were synthesized under 50°C and labeled with FITC. Then, Ab, a tumor-targeting ligand, was conjugated to the surface of CuS NPs. The morphology of CuS NPs and CuS-Ab NPs was evaluated by TEM, which clearly showed that these NPs were mono-dispersed and non-aggregating (Figure 2A and B). Furthermore, the DLS data showed that Ab was successfully bound to CuS NPs because the hydrodiameters had obviously changed after being doped with Ab (Figure 2C). The spectra of FITC-CuS NPs and FITC-CuS-Ab NPs showed a small peak at about 480 nm (Figure 2D), providing evidence that FITC-PEG2k-SH was loaded on to the surface of CuS NPs. Moreover, CuS-Ab NPs had a maximum wavelength at 1,065 nm, as recorded by the UV-3600 spectrophotometer, illustrating that these NPs had potential photothermal properties in the second NIR-II window. Meanwhile, the XRD spectra exhibited similar peaks between CuS NPs and CuS-Ab NPs (JCPDS no 06-0464), suggesting that the samples had negligible effects on the XRD spectra of NPs (Figure 2E).

Considering the absorption spectra, we investigated further the photothermal efficiency and photothermal stability of CuS-Ab NPs after exposure to a 1,064 nm laser in vitro (Figure 2F and H). The quartz cells filled with sample solution were irradiated by a 1,064 nm laser (0.2 W/cm^2) and thermal images were monitored in real time by an IR thermal camera. After 10 minutes, the color had notably changed in the quartz cell, as the temperature rapidly increased from 23°C to 58°C. In contrast, the 1,064 nm laser did not cause the temperature to rise sharply in the PBS group, which meant less damage to normal tissue under the same conditions. Furthermore, the stability of CuS-Ab NPs was evaluated by multiple exposure to a 1,064 nm laser in vitro. After five cycles, the maximum temperature of CuS-Ab NPs was kept at 58°C, demonstrating the surprisingly high photothermal stability (Figure 2G). Importantly, the dispersity of CuS NPs solution did not noticeably change after modification with FITC-PEG2k-SH or with Ab (Figure 2I). In addition, the stability of samples was demonstrated at 4°C for 1 month (Figure S1). Taken together, all these results show that CuS-Ab NPs can be feasibly applied both in vitro and in vivo.

In vitro cytotoxicity

Taking advantage of the photothermal properties of NPs, we compared and investigated the cytotoxicity of CuS NPs and CuS-Ab NPs in vitro. Here, 4T1 cells were cultured into 96-well plates and the MTT assay was used to assess the cytotoxicity of CuS-Ab NPs. As shown in Figure 3C, the viability of CuS-Ab NPs with laser irradiation decreased to 42%±2% at 40 μg/mL and 78%±8% at 10 μg/mL, indicating that apoptosis was induced in a concentration-dependent manner. Without laser irradiation, the cell viability of the CuS-Ab NPs group was 62%±5% at 40 μg/mL, and as high as 90%±5% at 10 μg/mL. In contrast, there was no notable reduction in cell viability in the control, laser-only group, or the CuS NPs-only group, indicating that 4T1 presented a high level of tolerance when cells were treated with only the laser or only CuS NPs.

Furthermore, flow cytometry was performed to evaluate cell viability. 4T1 cells (1×10^4 cells per well) were seeded into six-well plates at 37°C and 5% CO_2, and irradiated by a 1,064 nm laser (0.2 W/cm^2, 10 minutes). In Figure 3A, the treatment group (CuS-Ab NPs + laser group, CuS NPs + laser group, CuS NPs + Ab + laser group) exhibited lower cell viability than the control group (untreated group, laser-only

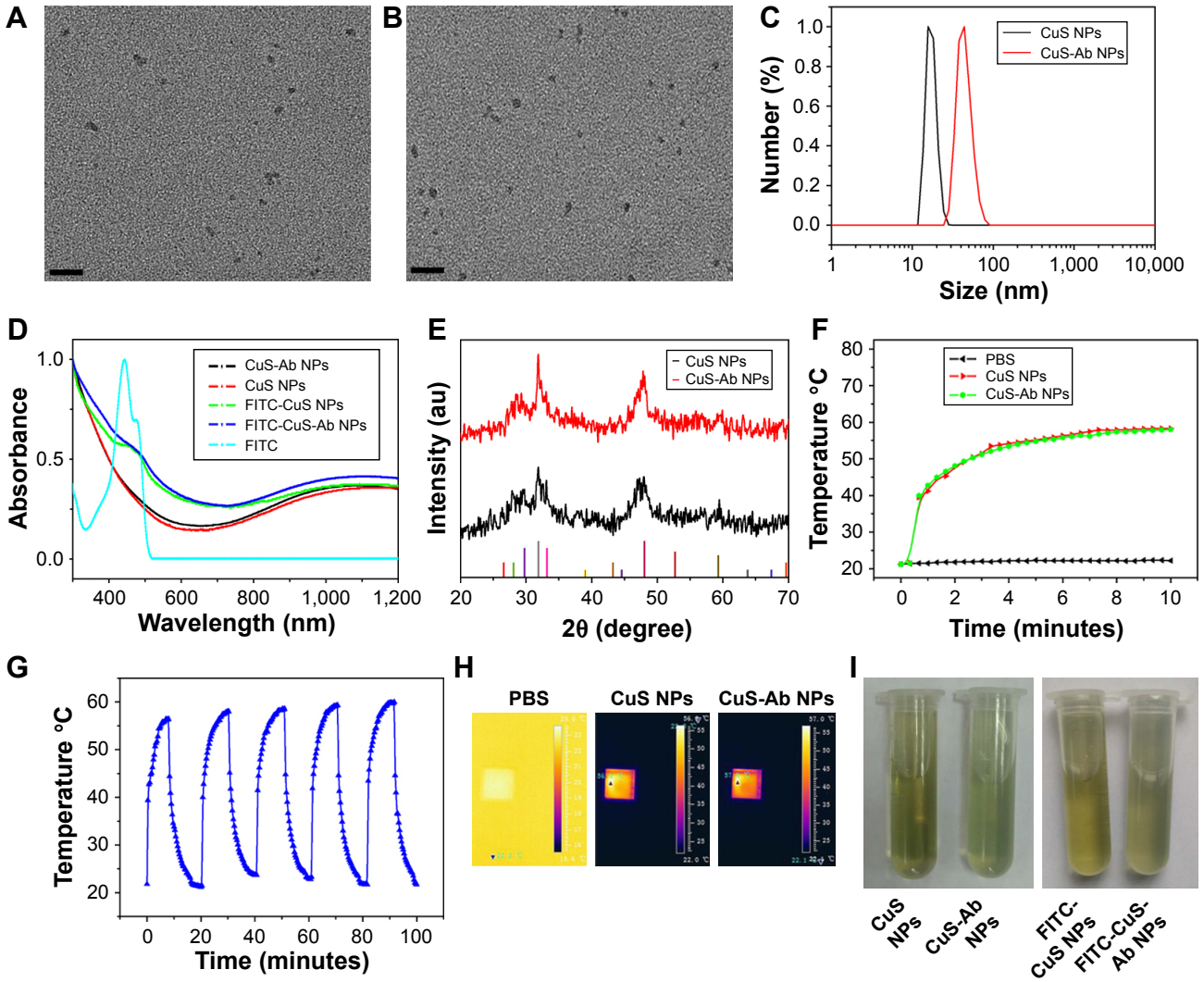

Figure 2 Characterization of targeted CuS NPs.

Notes: (**A**) TEM of CuS NPs (scale bar: 50 nm). (**B**) TEM of CuS-Ab NPs (scale bar: 50 nm). (**C**) DLS of CuS NPs and CuS-Ab NPs. (**D**) Absorbance spectra of CuS NPs, CuS-Ab NPs, FITC-CuS NPs, FITC-CuS-Ab NPs, and FITC. (**E**) XRD spectra of CuS NPs and CuS-Ab NPs. (**F**) Rising temperature curve of CuS NPs and CuS-Ab NPs under irradiation with a 1,064 nm laser (0.2 W/cm^2, 10 minutes). (**G**) Rising temperature curve of CuS-Ab NPs within five cycles under irradiation with a 1,064 nm laser (0.2 W/cm^2, 10 minutes). (**H**) Thermal images of PBS, CuS NPs, and CuS-Ab NPs in a quartz cell. (**I**) Dispersity of CuS NPs, CuS-Ab NPs, FITC-CuS NPs, and FITC-CuS-Ab NPs.

Abbreviations: CuS NP, CuS nanoparticle; CuS-Ab NP, cetuximab-modified CuS NP; DLS, dynamic light scattering; FITC, fluorescein isothiocyanate; TEM, transmission electron microscopy; XRD, X-ray diffraction.

group, and CuS NPs-only group). The CuS-Ab NPs + laser group (40 μg/mL, based on copper ions) demonstrated the lowest cell viability, indicating the stronger toxicity of Ab-functionalized CuS NPs combined with PTT.

In addition, calcein AM/PI co-staining was utilized to confirm the outcome of PTT. As shown in Figure 3B, the control group emitted a homogeneous green color indicative of living cells, while the treatment group exhibited a red color indicative of dead cells, which was consistent with the results of the MTT assay and flow cytometry, demonstrating that CuS-Ab NPs combined with PTT could improve the efficiency of tumor therapy.

Cellular uptake

It is known that Ab can directly target 4T1 cells owing to the EGFR being abnormally activated and overexpressed. To illustrate the selective targeting of CuS-Ab NPs, we compared and estimated cellular uptake of targeted NPs (CuS-Ab NPs) and untargeted nanoparticles (CuS NPs) in vitro. In Figure 3E, strong green fluorescence was emitted from FITC-labeled NPs, which is indicative of endocytosis. By co-staining with LysoTracker Green and DAPI, the red regions indicative of lysosomes and blue regions indicative of cell nuclei were observed by a laser scanning confocal microscope. The CuS-Ab NPs were internalized by 4T1 cells

more than were CuS NPs owing to the high affinity between Ab and EGFR, resulting in stronger green fluorescence. In merged images, the yellow color, which indicates overlay regions, in the CuS-Ab NPs group was brighter than in the CuS NPs group, indicating that CuS-Ab NPs enter the 4T1 cells through lysosomes.

Scratch test and anti-angiogenesis in vitro

Considering the anti-angiogenesis properties of Ab, we speculated that CuS-Ab NPs could have anti-vessel properties in tumor therapy.[38] Therefore, the migration efficiency of HUVECs and vessel growth models (chick ECM) were employed to probe and evaluate the anti-angiogenic potential

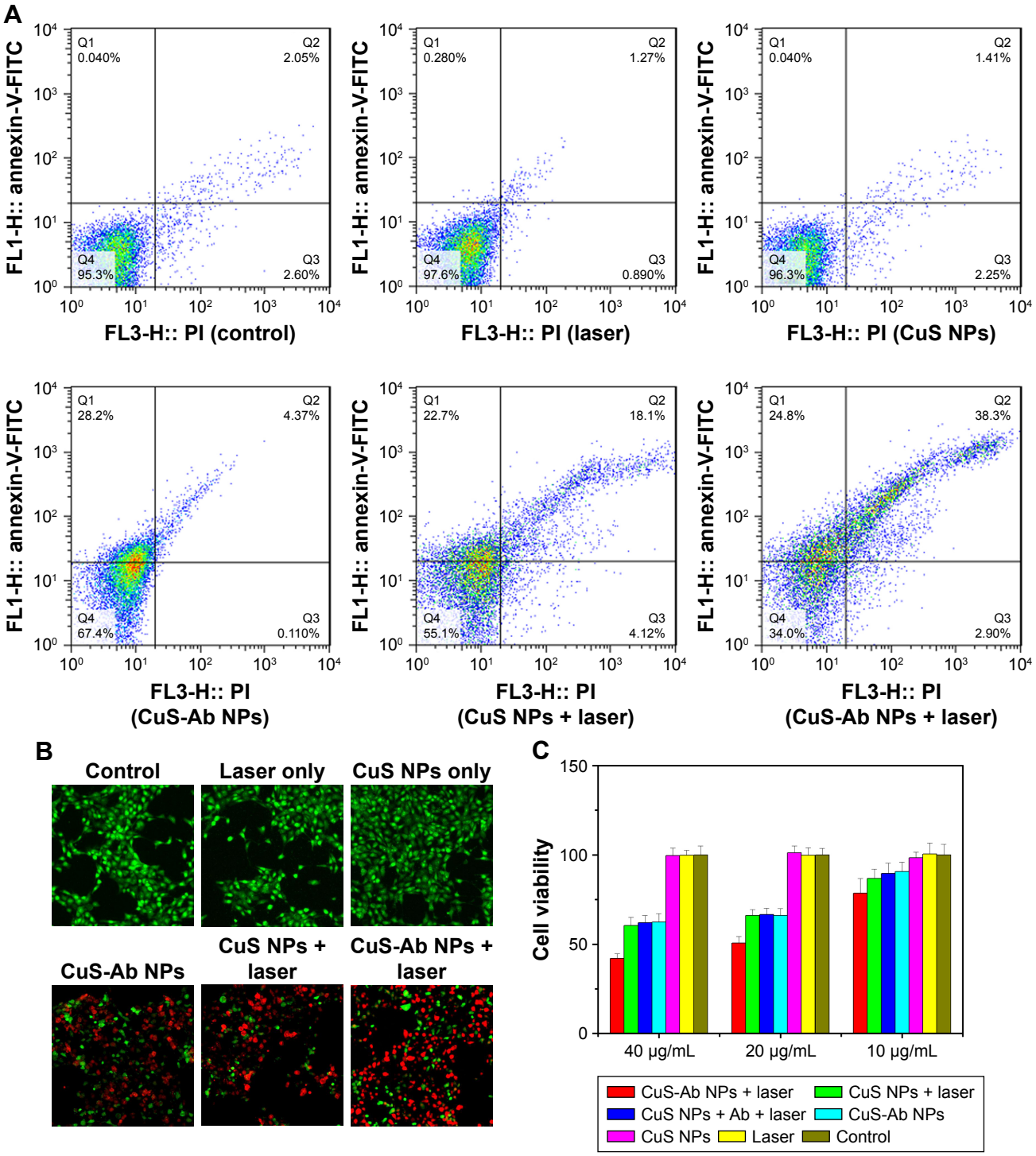

Figure 3 (*Continued*)

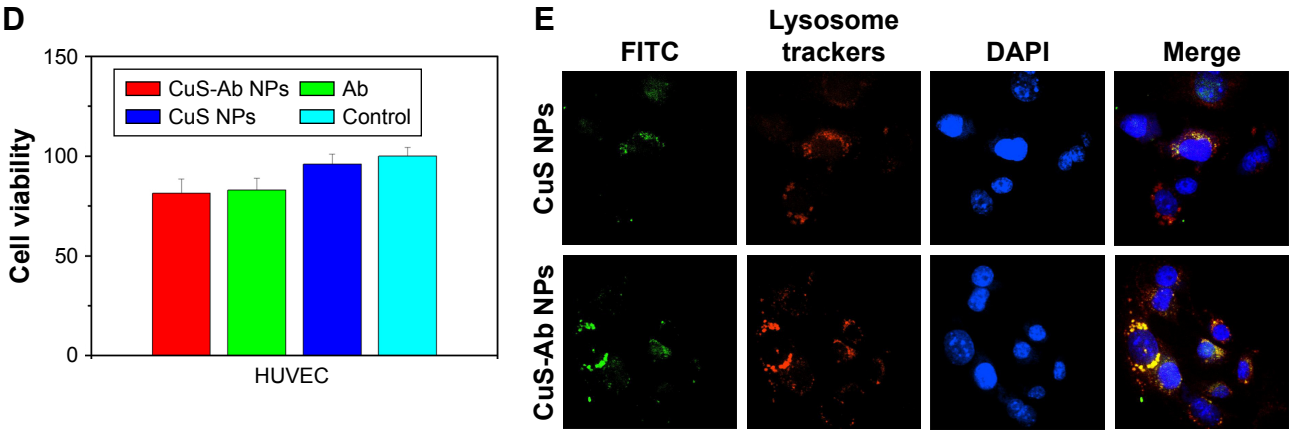

Figure 3 Cytotoxicity and cellular uptake of CuS NPs in vitro.

Notes: (**A**) The cytotoxicity of NPs was evaluated by flow cytometry after co-culture with 4T1 cells. (**B**) Cell viability in each group was evaluated by calcein AM/PI co-staining with or without 1,064 nm laser irradiation (magnification: 40× objective; calcein AM, green indicates living cells; PI, red indicates dead cells). (**C**) Viability of 4T1 cells in all groups with or without CuS NPs at different concentrations in the presence or absence of irradiation. (**D**) Viability of HUVECs was assessed by MTT without laser irradiation. (**E**) Cellular uptake of CuS NPs and CuS-Ab NPs was observed by laser scanning confocal microscopy (60×, oil objective). Green indicates FITC-CuS NPs and FITC-CuS-Ab NPs; red indicates lysosomes; blue indicates cell nuclei. All data represent mean values (n=3).

Abbreviations: calcein AM, calcein-acetoxymethyl ester; CuS NP, CuS nanoparticle; CuS-Ab NP, cetuximab-modified CuS NP; FITC, fluorescein isothiocyanate; HUVEC, human umbilical vein endothelial cell; PI, propidium iodide.

of CuS-Ab NPs. First, we evaluated the toxicity of CuS-Ab NPs to HUVECs by the MTT assay. From Figure 3D, there was no remarkable reduction in cell viability in the CuS-Ab NPs group (10 μg/mL), even with irradiation (1,064 nm, 0.2 W/cm^2, 10 minutes), indicating negligible cell toxicity of CuS-Ab NPs at low doses. Second, the monolayer of HUVECs was seeded in six-well plates and wounded by a sterile pipette tip. After 24 hours' stimulation of NPs (10 μg/mL), the scratch region of HUVECs disappeared in the control group and the CuS NPs group, indicating that CuS NPs alone were highly biocompatible and did not inhibit migration (Figure 4A and B). In contrast, the CuS-Ab NPs group and CuS NPs + Ab group still exhibited obvious wounds, supporting that CuS-Ab NPs had anti-angiogenic potential, as did the CuS NPs + Ab group. We further investigated and compared the anti-angiogenesis of CuS-Ab NPs in vessel growth models (chick ECM) under pathogen-free conditions (37°C and 70% humidity for 1 week). The results also showed less neovascularization in the CuS-Ab NPs group than in the control, indicating that CuS-Ab NPs had outstanding anti-tumor efficiency (Figure 4C and D).

Accumulation of targeting NPs in tumor

Encouraged by the cellular uptake of CuS-Ab NPs in vitro, xenograft tumor models were built and the targeted tumor efficiency was further surveyed. The tumor-bearing mice were injected intravenously with CuS NPs and CuS-Ab NPs. According to Figure 5A, FITC-CuS-Ab NPs could home to the 4T1 tumor owing to Ab having high affinity with EGFR, with the result that the red fluorescence of FITC-CuS-Ab NPs was brighter than that of FITC-CuS NPs. Based on this result, we further observed and compared the fluorescence intensity of a series of organs in vitro using an imaging system (Figure 5C and D). There was a striking difference between FITC-CuS-Ab NPs and FITC-CuS NPs. Compared with the FITC-CuS NPs group, the fluorescence intensity of tumor was continuously elevated while the fluorescence intensity of liver constantly declined in the FITC-CuS-Ab NPs group, reflecting the superior tumor targeting. The targeting efficacy was further demonstrated by the semi-quantitative analysis of FITC-labeled NPs in major tissues (Figure 5B). After the dissection and collection of tumors and normal tissues, fluorescence imaging was also conducted. As indicated in Figure 5C and D, we can more intuitively and visually find that after the modification with Ab, CuS NPs acquire a targeting capability and are more easily captured by the tumor.

In vivo anti-tumor efficacy

On the basis of the photothermal properties in vitro, the temperature of CuS-Ab NPs was investigated in vivo under a 1,064 nm laser (0.2 W/cm^2, 10 minutes). An IR camera was used to monitor the temperature of 4T1 xenograft mice at 24 hours after intravenous injection. In Figure 6A, the temperature increased rapidly in both treatment groups (CuS NPs group and CuS-Ab NPs group), while the

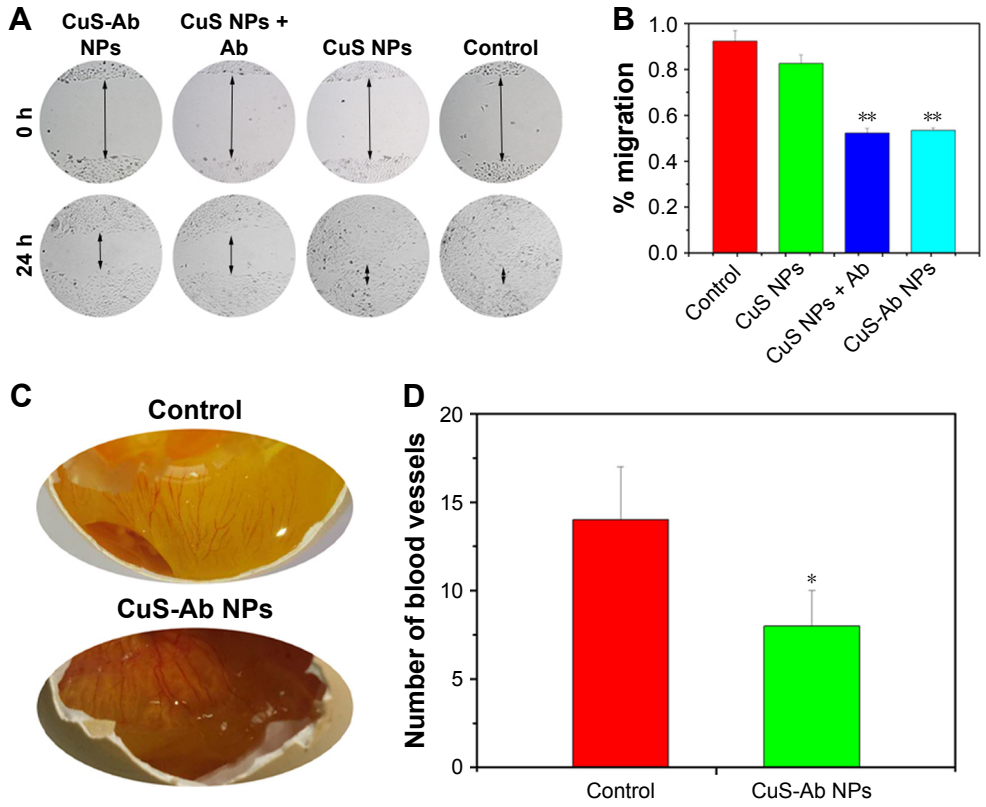

Figure 4 Scratch test and anti-angiogenesis effect in vitro.
Notes: (**A**) Representative images of the scratch test after co-incubation of HUVECs with CuS NPs, CuS NPs + Ab and CuS-Ab NPs; control group: without treatment (magnification: 40× objective). (**B**) Semi-quantitative analysis of percentage migration. (**C**) Blood density of ECM after 1 week of treatment. (**D**) Semi-quantitative analysis of vessel density in ECM. *$P<0.05$, **$P<0.01$.
Abbreviations: CuS NP, CuS nanoparticle; CuS-Ab NP, cetuximab-modified CuS NP; ECM, embryo chorioallantoic membrane; HUVEC, human umbilical vein endothelial cell.

temperature changed slowly in the control group under the same conditions. In Figure 6B, the temperature was elevated rapidly to above 44°C in the treatment group within 5 minutes, indicating that CuS NPs were an outstanding photothermal agent.

In light of their targeting efficiency and anti-angiogenic potential, we further probed the anti-tumor efficacy in vitro of CuS-Ab NPs under irradiation with a 1,064 nm laser (0.2 W/cm^2, 10 minutes). The 4T1 xenograft mice were randomly divided into four groups and injected intravenously

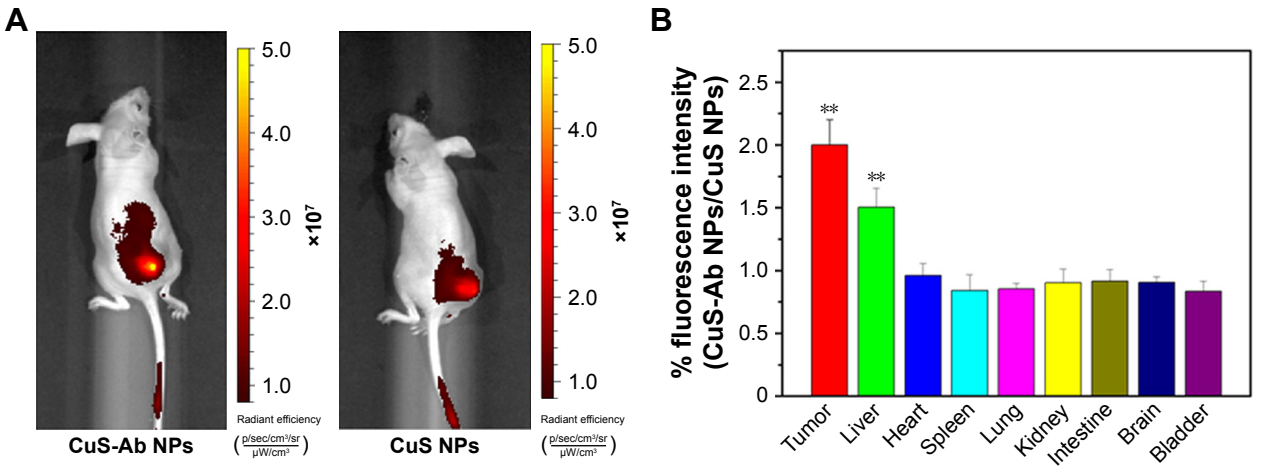

Figure 5 (*Continued*)

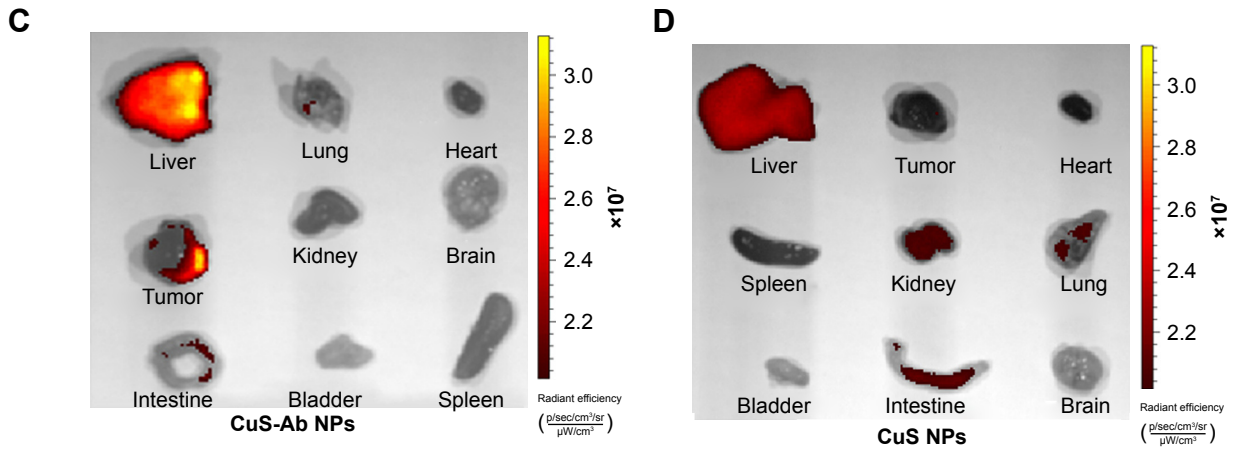

Figure 5 Fluorescence images of mice in vivo.
Notes: (**A**) Representative fluorescence images of NPs in vivo at 1 hour after intravenous injection of CuS-Ab NPs (left) and CuS NPs (right). The different colors indicate the intensity of fluorescence. (**B**) Semi-quantitative analysis of FITC-labeled NPs in major tissues. The fluorescence intensity ratio of CuS-Ab NPs to CuS NPs was assessed in major tissues after the mice had been killed. (**C, D**) Representative fluorescence images of CuS NPs and CuS-Ab NPs in major tissues. All data represent mean values (n=3). $^{**}P<0.01$.
Abbreviations: CuS NP, CuS nanoparticle; CuS-Ab NP, cetuximab-modified CuS NP.

with PBS (control), CuS NPs, CuS NPs + Ab, and CuS-Ab NPs, respectively. The length and width of the tumor and the weight of all mice were recorded every other day. The tumor volume increased rapidly after injecting PBS in the control group. In contrast, CuS NPs combined with irradiation with a 1,064 nm laser led to a slight inhibition of tumor development. CuS NPs in combination with Ab showed stronger inhibition of tumor growth under the same conditions. Surprisingly, after injection of Ab modified with CuS NPs, tumor volume growth was significantly delayed compared with CuS NPs + Ab groups under exposure to the laser within 2 weeks (Figure 6D and E). Moreover, the weights of mice were monitored every second day, and no notable differences between groups were seen during the treatment period (Figure 6C). Based on these phenomena, the results indicated that CuS NPs modified with a targeting ligand could enhance anti-tumor efficiency. Furthermore, IHC staining was used to assess the anti-angiogenic potential of CuS-Ab NPs in tumor tissue (Figure 6F). Compared to the control group, the CuS NPs displayed negligible neovascularization in tumor upon CD31 staining under a light microscope, while the CuS NPs + Ab and CuS-Ab NPs groups exhibited remarkable reductions in vessel density, implying that anti-tumor angiogenesis may be a reason for the anti-tumor growth characteristic of CuS-Ab NPs. In general, the targeting ligand was mainly used to enhance the accumulation of NPs into the tumor. For example, RGD was used to modify CuS NPs to increase the tumor targeting efficiency.[36] Nevertheless, Ab could also be used to inhibit tumor development through anti-angiogenesis.

Safety evaluation

H&E staining was used to evaluate preliminary safety after the tumor-bearing mice had been killed. Compared with control mice, no obvious damage was observed in the major organs (heart, liver, lung, spleen, and kidney) after treatment with CuS-Ab NPs for 2 weeks (Figure 7), providing evidence for the superior biocompatibility of the material in vivo.

Conclusion

In this contribution, we developed targeted CuS-Ab NPs to enhance efficacy and biosafety in 4T1 xenograft mice which overexpressed EGFR on tumor cell membranes. The CuS-Ab NPs exhibited excellent PTT efficacy after exposure with a 1,064 nm laser at low intensities, providing evidence for the enhancement of tumor ablation and minimization of normal tissue damage. The anti-tumor efficacy of CuS-Ab NPs was enhanced owing to tumor-homing ligand and anti-angiogenesis after the introduction of the targeting antibody. For first-round safety evaluation, there are no indications that the CuS-Ab NPs could trigger damage in major organs, such as disorganization and inflammatory lesions, which were assessed by H&E staining under light microscopy. On the basis of our results, we believe that highly biocompatible CuS-Ab NPs, as an ideal photothermal agent, have potential application in tumor therapy in the clinic.

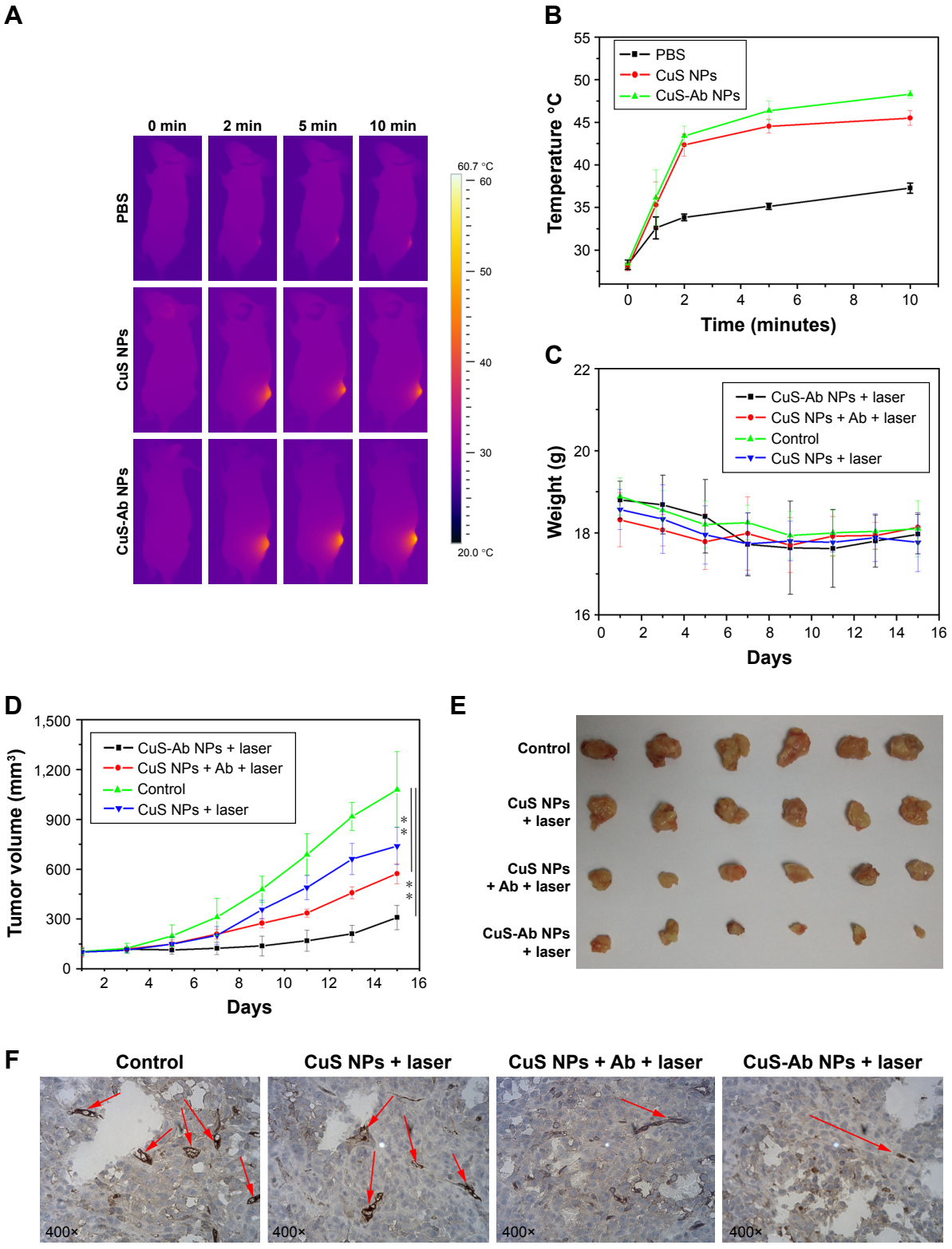

Figure 6 Thermal imaging and anti-tumor efficacy of PTT in vivo for 4T1 xenograft tumor mice.

Notes: (**A**) Representative thermal images of tumor under irradiation laser (0.2 W/cm^2, 10 minutes) after treatment with CuS NPs and CuS-Ab NPs. (**B**) Rising temperature curve of tumor in live mice after treatment with CuS NPs and CuS-Ab NPs. The control group was treated with PBS. (**C**) The weight of the mice was monitored every other day. (**D**) Tumor volume curve of xenograft tumor mice over 2 weeks. The tumor volume was calculated from the length and width of the tumor, obtained from live mice every other day. (**E**) Representative tumor images were obtained from live mice in different groups with or without treatment. (**F**) Immunohistochemistry staining of CD31 in tumor. The red arrow indicates CD31 in endothelial vessels. All data represent mean values (n=6). $^{**}P<0.01$.

Abbreviations: CuS NP, CuS nanoparticle; CuS-Ab NP, cetuximab-modified CuS NP; PTT, photothermal therapy.

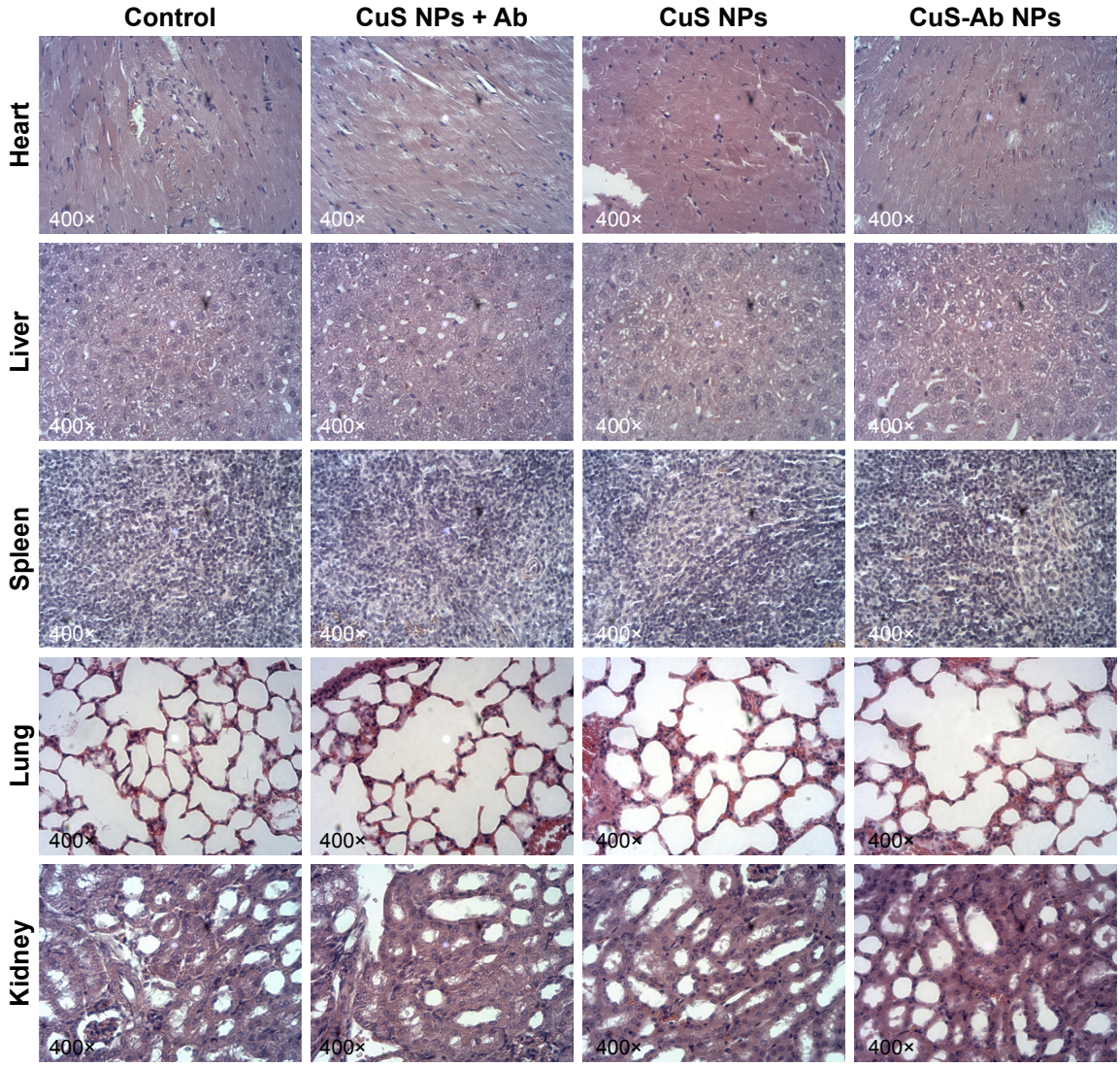

Figure 7 Light microscopy images of H&E-stained tissue sections (heart, liver, spleen, lung, and kidney).
Notes: The 4T1 xenograft tumor mice were treated with CuS NPs + laser, CuS NPs + Ab + laser and CuS-Ab NPs + laser for 2 weeks. Then, all mice were killed and major tissues were collected.
Abbreviations: CuS NP, CuS nanoparticle; CuS-Ab NP, cetuximab-modified CuS NP.

Acknowledgment

This study was supported by Nanjing University Innovation and Creative Program for PhD candidates (candidate 2016018).

Author contributions

All authors contributed to data analysis, drafting and revising the article, gave final approval of the version to be published, and agree to be accountable for all aspects of the work.

Disclosure

The authors report no conflicts of interest in this work.

References

1. Brannon-Peppas L, Blanchette JO. Nanoparticle and targeted systems for cancer therapy. *Adv Drug Deliv Rev*. 2012;64:206–212.
2. Honoré C, Amroun K, Vilcot L, et al. Abdominal desmoplastic small round cell tumor: multimodal treatment combining chemotherapy, surgery, and radiotherapy is the best option. *Ann Surg Oncol*. 2015;22(4):1073–1079.
3. Carmeliet P, Jain RK. Angiogenesis in cancer and other diseases. *Nature*. 2000;407(6801):249–257.
4. Ferrari M. Cancer nanotechnology: opportunities and challenges. *Nat Rev Cancer*. 2005;5(3):161–171.
5. Liu T, Shi S, Liang C, et al. Iron oxide decorated MoS2 nanosheets with double PEGylation for chelator-free radiolabeling and multimodal imaging guided photothermal therapy. *ACS Nano*. 2015;9(1):950–960.
6. Chen Q, Wang C, Cheng L, He W, Cheng Z, Liu Z. Protein modified upconversion nanoparticles for imaging-guided combined photothermal and photodynamic therapy. *Biomaterials*. 2014;35(9):2915–2923.
7. Cheng L, Wang C, Feng L, Yang K, Liu Z. Functional nanomaterials for phototherapies of cancer. *Chem Rev*. 2014;114(21):10869–10939.
8. Tang L, Zhang F, Yu F, et al. Croconaine nanoparticles with enhanced tumor accumulation for multimodality cancer theranostics. *Biomaterials*. 2017;129:28–36.

9. Jiang Y, Upputuri PK, Xie C, et al. Broadband absorbing semiconducting polymer nanoparticles for photoacoustic imaging in second near-infrared window. *Nano Lett*. 2017;17(8):4964–4969.
10. Ali MR, Rahman MA, Wu Y, et al. Efficacy, long-term toxicity, and mechanistic studies of gold nanorods photothermal therapy of cancer in xenograft mice. *Proc Natl Acad Sci U S A*. 2017;114(15): E3110–E3118.
11. Ali MRK, Wu Y, Tang Y, et al. Targeting cancer cell integrins using gold nanorods in photothermal therapy inhibits migration through affecting cytoskeletal proteins. *Proc Natl Acad Sci U S A*. 2017;114(28): E5655–E5663.
12. Liang C, Diao S, Wang C, et al. Tumor metastasis inhibition by imaging-guided photothermal therapy with single-walled carbon nanotubes. *Adv Mater*. 2014;26(32):5646–5652.
13. Liu J, Wang C, Wang X, et al. Mesoporous Silica Coated Single-Walled Carbon Nanotubes as a Multifunctional Light-Responsive Platform for Cancer Combination Therapy. *Adv Funct Mater*. 2015;25(3): 384–392.
14. Zc W, Wp L, Luo CH, et al. Rattle-type Fe3O4@CuS developed to conduct magnetically guided photoinduced hyperthermia at first and second NIR biological windows. *Adv Funct Mater*. 2015;25(41):6527–6537.
15. Zhang C, Ren J, Hua J, et al. Multifunctional Bi_2WO_6 Nanoparticles for CT-Guided Photothermal and Oxygen-free Photodynamic Therapy. *ACS Appl Mater Interfaces*. 2018;10(1):1132–1146.
16. Chen Y, Cheng L, Dong Z, et al. Degradable Vanadium Disulfide Nanostructures with Unique Optical and Magnetic Functions for Cancer Theranostics. *Angew Chem Int Ed Engl*. 2017;56(42):13171–13176.
17. Wang S, Riedinger A, Li H, et al. Plasmonic copper sulfide nanocrystals exhibiting near-infrared photothermal and photodynamic therapeutic effects. *ACS Nano*. 2015;9(2):1788–1800.
18. Guo L, Yan DD, Yang D, et al. Combinatorial photothermal and immuno cancer therapy using chitosan-coated hollow copper sulfide nanoparticles. *ACS Nano*. 2014;8(6):5670–5681.
19. Goel S, Chen F, Cai W. Synthesis and biomedical applications of copper sulfide nanoparticles: from sensors to theranostics. *Small*. 2014; 10(4):631–645.
20. Zhou M, Tian M, Li C, Min Z, Mei T. Copper-based nanomaterials for cancer imaging and therapy. *Bioconjug Chem*. 2016;27(5):1188–1199.
21. Zedan AF, Moussa S, Terner J, Atkinson G, El-Shall MS. Ultrasmall gold nanoparticles anchored to graphene and enhanced photothermal effects by laser irradiation of gold nanostructures in graphene oxide solutions. *ACS Nano*. 2013;7(1):627–636.
22. Yuan H, Fales AM, Vo-Dinh T. TAT peptide-functionalized gold nanostars: enhanced intracellular delivery and efficient NIR photothermal therapy using ultralow irradiance. *J Am Chem Soc*. 2012;134(28): 11358–11361.
23. Li M, Yang X, Ren J, Qu K, Qu X. Using graphene oxide high near-infrared absorbance for photothermal treatment of Alzheimer's disease. *Adv Mater*. 2012;24(13):1722–1728.
24. Lane LA, Xue R, Nie S. Emergence of two near-infrared windows for *in vivo* and intraoperative SERS. *Curr Opin Chem Biol*. 2018;45: 95–103.
25. Smith AM, Mancini MC, Nie S. Bioimaging: second window for *in vivo* imaging. *Nat Nanotechnol*. 2009;4(11):710–711.
26. Prodi L, Rampazzo E, Rastrelli F, Speghini A, Zaccheroni N. Imaging agents based on lanthanide doped nanoparticles. *Chem Soc Rev*. 2015; 44(14):4922–4952.
27. Hong G, Antaris AL, Dai H. Near-infrared fluorophores for biomedical imaging. *Nature Biomedical Engineering*. 2017;1:0010.
28. Li Q, Tang Q, Zhang P, et al. Human epidermal growth factor receptor-2 antibodies enhance the specificity and anticancer activity of light-sensitive doxorubicin-labeled liposomes. *Biomaterials*. 2015;57:1–11.
29. Baselga J. The EGFR as a target for anticancer therapy – focus on cetuximab. *Eur J Cancer*. 2001;37 Suppl 4:16–22.
30. Lu Q, Dai X, Zhang P, et al. Fe_3O_4@Au composite magnetic nanoparticles modified with cetuximab for targeted magneto-photothermal therapy of glioma cells. *Int J Nanomedicine*. 2018;13:2491–2505.
31. Shih YH, Luo TY, Chiang PF, et al. EGFR-targeted micelles containing near-infrared dye for enhanced photothermal therapy in colorectal cancer. *J Control Release*. 2017;258:196–207.
32. Ferguson HJ, Wragg JW, Ward S, Heath VL, Ismail T, Bicknell R. Glutamate dependent NMDA receptor 2D is a novel angiogenic tumour endothelial marker in colorectal cancer. *Oncotarget*. 2016;7(15): 20440–20454.
33. Salierno MJ, García AJ, Del Campo A. Photoactive Biomaterials: Photo-Activatable Surfaces for Cell Migration Assays (Adv. Funct. Mater. 48/2013). *Adv Funct Mater*. 2013;23(48):5974–5980.
34. Liu Z, Liu J, Wang R, et al. An efficient nano-based theranostic system for multi-modal imaging-guided photothermal sterilization in gastrointestinal tract. *Biomaterials*. 2015;56:206–218.
35. Roma-Rodrigues C, Heuer-Jungemann A, Fernandes AR, Kanaras AG, Baptista PV. Peptide-coated gold nanoparticles for modulation of angiogenesis *in vivo*. *Int J Nanomedicine*. 2016;11:2633–2639.
36. Shi H, Yan R, Wu L, et al. Tumor-targeting CuS nanoparticles for multimodal imaging and guided photothermal therapy of lymph node metastasis. *Acta Biomater*. 2018;72:256–265.
37. Chen LJ, Sun SK, Wang Y, Yang CX, Wu SQ, Yan XP. Activatable multifunctional persistent luminescence nanoparticle/copper sulfide nanoprobe for *in vivo* luminescence imaging-guided photothermal therapy. *ACS Appl Mater Interfaces*. 2016;8(48):32667–32674.
38. Droller MJ. Anti-epidermal growth factor receptor antibody C225 inhibits angiogenesis in human transitional cell carcinoma growing orthotopically in nude mice. *J Urol*. 2000;164(2):594.

Supplementary material

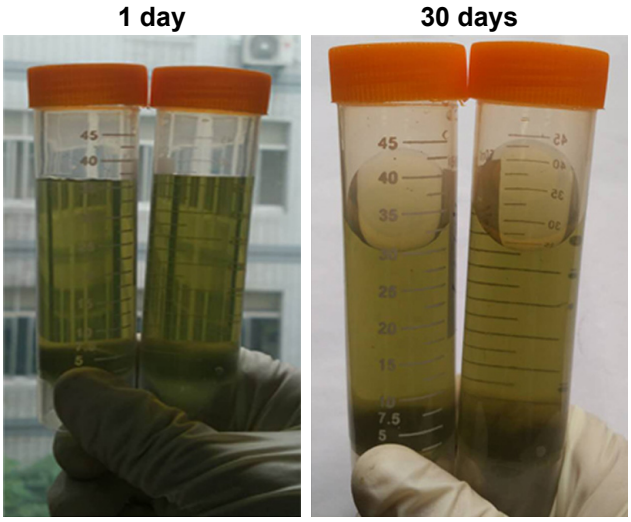

Figure S1 Long-term stability of CuS NPs and CuS-Ab NPs.
Notes: The samples were kept at 4°C for 1 month. The color of the samples did not change.
Abbreviations: CuS NP, CuS nanoparticle; CuS-Ab NP, cetuximab-modified CuS NP.